BULLETIN OF THE POLISH ACADEMY OF SCIENCES
TECHNICAL SCIENCES
DOI: 10.24425/bpasts.2024.151953

THIS IS AN EARLY ACCESS ARTICLE.
This article has been accepted for publication in a future issue of this journal, but has not been fully edited. Content may change prior to final publication.

A Sustainable Approach-based Optimization of Internal Diamond Burnishing Operation

An-Le Van[1], Truong-An Nguyen[2], Xuan-Ba Dang[3], Trung-Thanh Nguyen[2*]

[1]Faculty of Engineering and Technology, Nguyen Tat Thanh University, 300A Nguyen Tat Thanh, Ho Chi Minh City 700000, Vietnam

[2]Faculty of Mechanical Engineering, Le Quy Don Technical University, 236 Hoang Quoc Viet, Ha Noi 100000, Viet Nam

[3]Department of Automatic Control, Ho Chi Minh City University of Technology and Education, 1 Vo Van Ngan Street, Linh Chieu Ward, Thu Duc City, Ho Chi Minh City 700000, Vietnam

Abstract. The related works of the diamond burnishing processes focused on improvements in surface quality. The study aims to optimize burnishing factors, including the spraying distance of the nozzle (*S*), the inlet pressure of the cold air (*I*), and the quantity of the liquid CO_2 (*L*) of the cool and cryogenic-assisted diamond burnishing operation for minimizing energy consumed (*EC*) and arithmetical mean surface height roughness (*Sa*). Burnishing responses are modeled based on the radial basis function network and full factorial data. The entropy method, improved grey wolf optimizer, non-dominated sorting genetic algorithm II, and technique for order of preference by similarity to ideal solution were implemented to calculate the weights, produce solutions, and select the best outcome. As a result, the optimal data of the *S*, *I*, and *L* were 15.0 mm, 3.0 bar, and 11.0 L/min, respectively. The *Sa* and *EC* were reduced by 20.4% and 3.8%, respectively, at the optimality. The optimized outcomes could be employed to improve energy efficiency and machining quality for the internal diamond burnishing process. The optimizing technique could be used to solve complicated issues for different burnishing operations. The cool and cryogenic-assisted diamond burnishing process could be utilized for machining different internal holes.

Key words: internal burnishing; cryogenic CO_2; energy consumed; surface roughness; optimization

1. INTRODUCTION

The diamond burnishing process is renowned for its ability to produce a glossy surface finish with minimized friction. It offers additional benefits, such as a hardened surface layer for enhanced wear resistance and a compact surface topology that provides improved chemical resistance. The diamond tip smooths and polishes the surface when pressure is applied, reducing the need for additional finishing operations such as honing and polishing. Consequently, diamond burnishing operations can be considered a cost-effective method for machining ferrous and nonferrous materials.

Various burnishing processes have been considered and optimized to boost technical performances. A set of experiments of the burnished GCR15 steel was conducted to investigate the fatigue performance [1]. The authors indicated that the fatigue strength was increased by 36%, as compared to the non-burnished case. The surface properties of the burnished butt joints of the 2024 aluminum alloy were investigated by Kluz et al. The results revealed that the surface roughness and Vickers hardness were enhanced by 73.8% and 84.2%, respectively, with the aid of the diamond burnishing operation [2]. The MQL-assisted burnishing operation was developed to facilitate the external surface [3]. The authors stated that the total carbon emission and the roughness of the external diamond burnishing operation were reduced by 3.8% and 11.6% with the aid of the Taguchi method. Sachin et al. demonstrated that the ideal spindle speed, feed rate, and burnishing force could be used to achieve the surface roughness of 0.2 µm and Vickers hardness of 397.5 HV for the cryogenic burnished 17-4 steel [4]. The impacts of the burnishing speed, feed, and force on the surface properties of 42CrMo4 hard-turned steel were explored [5]. The authors presented that the force was the most dominant factor and the Vickers hardness was enhanced by 51.0%. A FEM model was developed to predict the roughness of the burnished surface [6]. The small errors between the simulated and actual data

* e-mail: trungthanhnguyen@lqdtu.edu.vn

This article has been accepted for publication in a future issue of this journal, but has not been fully edited. Content may change prior to final publication.

indicated the effectiveness of the proposed model. The Kriging models of the coefficient of friction, energy efficiency, and specific wear rate were developed in terms of the burnishing factors [7]. The authors stated that the responses were primarily affected by the burnishing speed and depth. Maximov et al. presented that the fatigue limit of the burnished 304 steel could be improved by 36.4%, as compared to untreated specimens [8]. A new burnishing tool was developed to enhance the wear corrosion of the burnished cylinder [9]. The authors presented that the wear rate of the specimen was reduced by 68.2%, as compared to un-burnished case. A multi-objective optimization was carried out using the desirability function for the sliding burnishing AISI 52100 steel [10]. The results revealed that the surface roughness and Vickers hardness were improved by 92% and 117%, respectively, while the fatigue life was increased up to 120%. A simulation model using the Cowper–Symonds coefficients was proposed to effectively predict the stress and deformation of the burnished 41Cr4 steel [11].

As a result, various diamond burnishing operations with MQL and cryogenic conditions have been developed. However, a novel diamond burnishing process comprising the cryogenic CO_2 and Vortex tube has not been developed. The proposed operation can be considered as a sustainable burnishing process due to the elimination of any lubricants. The *EC* and *Sa* models regarding cooling parameters have not been proposed for the internal diamond burnishing process. The optimal cooling parameters have not been selected to reduce the *EC* and *Sa*. Moreover, the cool and cryogenic-assisted burnishing process of the chromium-molybdenum steel (SCM440) has not been proposed [12].

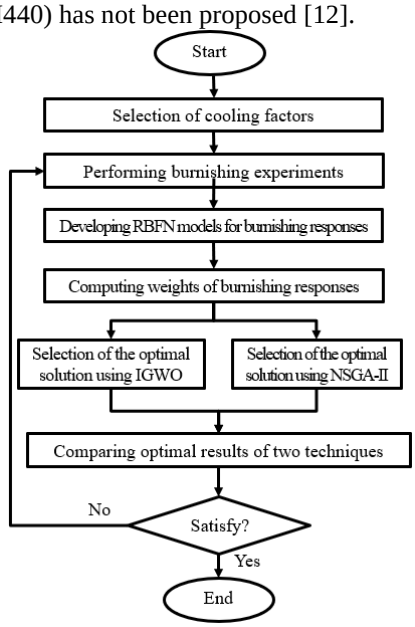

Fig. 1. Optimization approach

2. OPTIMIZATION APPROACH

In this work, the *EC* and *Sa* of the cool and cryogenic-assisted diamond burnishing operation are minimized by selecting optimal spraying distance, inlet pressure, and CO_2 quantity. The radial basis function network (RBFN) is used to develop the response models. The entropy method, improved grey wolf optimizer (IGWO), non-dominated sorting genetic algorithm II (NSGA II), and technique for order of preference by similarity to ideal solution (TOPSIS) are employed to calculate the weights, produce solutions, and select the best outcome.

The *Sa* is computed as:

$$Sa = \frac{\sum_{i=1}^{5} Sa_i}{5} \tag{1}$$

where Sa_i is arithmetical mean surface height roughness at the measured location, respectively.

The *EC* is computed as:

$$EC = \sum_{i=1}^{10} P_{mi} \times t_m \tag{2}$$

where P_{mi} and t_m are the power consumed at the i_{th} time and machining time, respectively.

The cooling parameters, including the *S*, *I*, and *L* are presented in Table 1. The ranges of each factor are determined based on the characteristics of the Vortex tube and CO_2 storage tank. These values are confirmed by related works and burnishing experts. The experimental values of the spindle speed, feed rate, and depth of penetration are 630 rpm, 0.05 mm/rev, and 0.06 mm, respectively.

The optimizing approach is presented in Fig. 1:

Step 1: Performing burnishing experiments [13].

Step 2: Developing RBFN models for responses [14].

TABLE 1. Diamond burnishing factors

Symbol	Cooling factors	Values
S	Spraying distance of the nozzle (mm)	15.0-25.0-35.0
I	Inlet pressure of the cold air (bar)	2.0-4.0-6.0
L	Quantity of the liquid CO_2 (L/min)	4.0-8.0-12.0

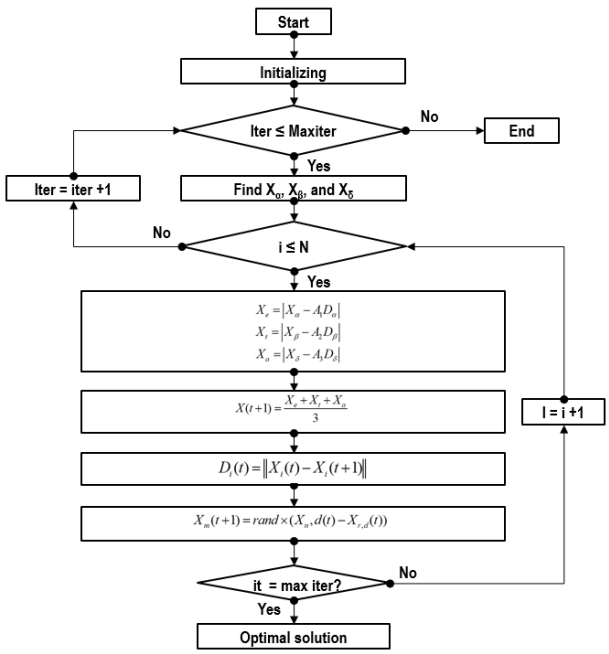

Fig. 2. The operating steps of the IGWO

This article has been accepted for publication in a future issue of this journal, but has not been fully edited. Content may change prior to final publication.

Fig. 3. Experiments of the diamond burnishing operation

The RBFN is utilized to present experimental data with the aid of the gaussian function. RBFN is a special type of the feed-forward neural network with three layers, including the input, hidden layer, and output. The network receives an n-dimensional input vector, while the Euclidean distance between the input vector and each neuron's center is computed at the hidden layer. The output node is used to calculate a score based on a weighted sum of the activation values from the hidden layer and expressed as:

$$out_i = \exp(-\frac{1}{2\sigma^2}\|s - c_i\|^2) \tag{3}$$

The gaussian function is expressed as:

$$\Phi(r) = \exp(-\gamma r^2) \tag{4}$$

where γ is a parameter, which is computed at the cross-validation stage.

The RBFN model for a given input is expressed as:

$$out = w_0 + \sum_{i=1}^{m} w_i \exp(-\frac{1}{2\sigma^2}\|s - c_i\|^2) \tag{5}$$

where w_0 and w_m are the bias and weight, respectively.

Step 3: Computing the weight of each response.

The normalized response (n_{ij}) is computed as:

$$n_{ij} = \frac{r_{ij}}{\sum_{i=1}^{m} r_{ij}} \tag{6}$$

The entropy value (e_j) of each response is computed as:

$$e_j = -\frac{\sum_{j=1}^{m} n_{ij} \times \ln n_{ij}}{\ln m} \tag{7}$$

The weight (ω_i) is computed as:

$$\omega_i = \frac{1 - e_j}{\sum_{j=1}^{n}(1 - e_j)} \tag{8}$$

Step 4: Selecting the bets optimal solution using the IGWO and TOPSIS.

In this work, the IGWO is proposed with the setting, evolution, and generation stages (Fig. 2).

In the setting stage, the wolves are distributed in the search space and expressed as:

$$X_{ij} = l_j + rand_j \times (u_j - l_j) \tag{9}$$

where $X_i(t)$ is the position of the i_{th} wolf. l_j and u_j are the given ranges.

In the evolution stage, an individual is learned by its different neighbors. A radius $D_i(t)$ is calculated using Euclidean distance between the current position of $X_i(t)$ and the candidate position $X_i(t+1)$ and expressed as:

$$D_i(t) = \|X_i(t) - X_i(t+1)\| \tag{10}$$

The neighbor ($N_i(t)$) is expressed as:

$$N_i(t) = \{X_j(t) | D_i(X_i(t), X_j(t)) \le R_i(t)\} \tag{11}$$

A prominent candidate $X_m(t+1)$ is expressed as:

$$X_m(t+1) = rand \times (X_n, d(t) - X_{r,d}(t)) \tag{12}$$

where $X_{r,d}(t)$ is a random wolf from the whole population.

The normalized solution (p_{ij}) is computed as [15]:

$$p_{ij} = \frac{x_{ij}}{\sqrt{\sum_{i=1}^{m} x_{ij}}} \tag{13}$$

A set of positive solution (S^+) is expressed as:

$$S_i^+ = \sqrt{\sum_{j=1}^{m}(p_{ij} - p_j^+)^2} \tag{14}$$

A set of positive solution (S^-) is expressed as:

$$S_i^- = \sqrt{\sum_{j=1}^{m}(p_{ij} - p_j^-)^2} \tag{15}$$

The evaluation indicator (E_I) is expressed as:

$$E_I = \frac{S_i^-}{S_i^+ + S_i^-} \tag{16}$$

3. EXPERIMENTAL FACILITIES

The burnishing trails are executed using a conventional lathe (Fig. 3). The 42CrMo4 steel is used to produce specimens due to its extensive usage in gears, engine shafts, and mold bushes. The length, internal diameter, and outer diameter of each specimen are 62 mm, 46 mm, and 56 mm, respectively. The drilling and internal turning operations are used to generate the hole. The cold air and cryogenic lubricant are produced from a Vortex tube and CO_2 tank, respectively. The burnishing device is clamped on the tool post. The burnishing length of 30 mm is conducted for all tests. The *Sa* of the initial surfaces is 4.632 µm. A new diamond tip is utilized after each burnishing trial.

The *Sa* values and power consumed are captured using the ZeGage Pro 3D optical profiler and Kyoritsu 6315 meter, respectively. The experimental results of No. 8 and 9 are depicted in Fig. 4.

4. RESULTS AND DISCUSSIONS

The experimental results of the burnishing trials are exhibited in Table 2.

This article has been accepted for publication in a future issue of this journal, but has not been fully edited. Content may change prior to final publication.

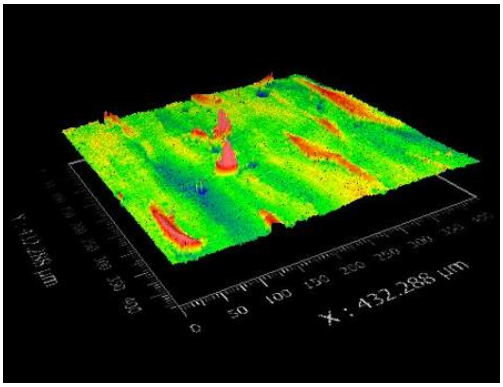

(a) *Sa* values at the experimental No. 8

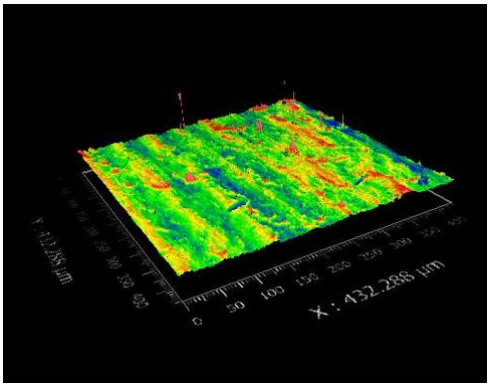

(b) *Sa* values at the experimental No. 9

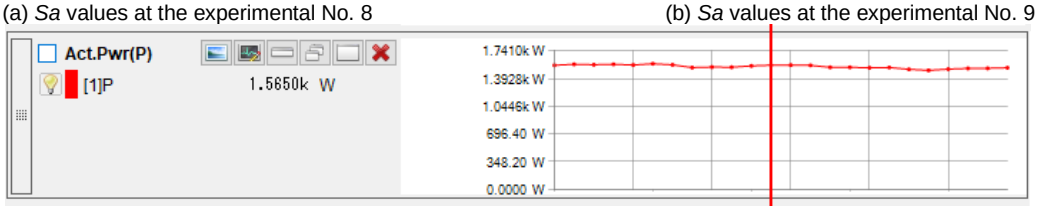

(c) The power consumed at the experimental No. 8

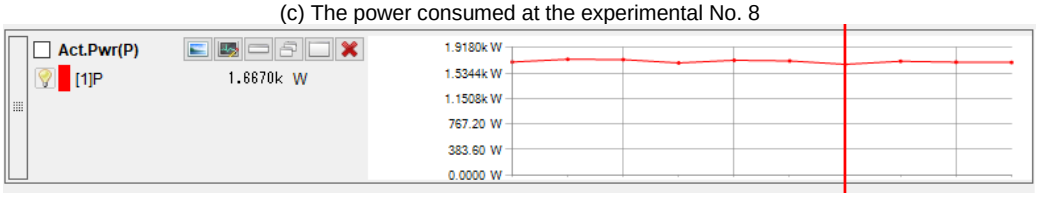

(d) The power consumed at the experimental No. 9

Fig. 4. Example results of the burnishing process

4.1. ANOVA analysis

The ANOVA results for the *Sa* model are shown in Table 3 [16, 17, 18]. The R^2 value of 0.9834 indicates that the developed model is significant. As a result, the contributions of the *S*, *I*, and *L* are 17.52%, 21.78%, and 25.51%, respectively (Fig. 5a). The contributions of the *SI*, *SL*, and *IL* are 5.55%, 8.33%, and 3.89%, respectively. The contributions of the S^2, I^2, and L^2 are 8.88%, 3.33%, and 5.21%, respectively.

The ANOVA results for the *EC* model are shown in Table 4. The R^2 value of 0.9846 indicates that the developed model is significant. As a result, the contributions of the *S*, *I*, and *L* are 23.19%, 30.63%, and 33.81%, respectively Fig. 5b). The contributions of the *SI*, *SL*, and *IL* are 2.71%, 2.27%, and 1.77%, respectively. The contributions of the S^2 and L^2 are 2.83% and 2.05%, respectively.

As shown in Figs. 6 a and b, the data are distributed on straight lines; hence, the developed RBFN models are adequate.

Table 5 presents the comparisons between the actual and RBFN-predicted outcomes. The slight variations (less than 5%) demonstrated that the RBFN models could be used to accurately predict burnishing responses.

TABLE 2. Experimental outcomes for the diamond burnishing operation

No.	*S* (mm)	*I* (bar)	*L* (L/min)	*Sa* (µm)	*EC* (kJ)
Data for developing RBFN models					
1	15.0	2.0	4.0	0.647	60.42
2	15.0	2.0	8.0	0.492	65.83
3	15.0	2.0	12.0	0.377	70.72
4	15.0	4.0	4.0	0.576	65.28
5	15.0	4.0	8.0	0.401	70.47
6	15.0	4.0	12.0	0.271	75.11
7	15.0	6.0	4.0	0.535	69.95
8	15.0	6.0	8.0	0.342	74.91
9	15.0	6.0	12.0	0.195	79.31
10	25.0	2.0	4.0	0.674	64.62
11	25.0	2.0	8.0	0.554	69.75
12	25.0	2.0	12.0	0.479	74.31
13	25.0	4.0	4.0	0.577	69.13
14	25.0	4.0	8.0	0.441	74.02
15	25.0	4.0	12.0	0.347	78.34
16	25.0	6.0	4.0	0.511	73.44
17	25.0	6.0	8.0	0.356	78.09
18	25.0	6.0	12.0	0.246	82.18
19	35.0	2.0	4.0	0.783	68.07
20	35.0	2.0	8.0	0.697	72.89
21	35.0	2.0	12.0	0.662	77.14
22	35.0	4.0	4.0	0.659	72.22
23	35.0	4.0	8.0	0.559	76.79
24	35.0	4.0	12.0	0.504	80.81
25	35.0	6.0	4.0	0.567	76.15
26	35.0	6.0	8.0	0.454	80.49
27	35.0	6.0	12.0	0.377	84.27
Data for testing accuracy of RBFN models					
28	18.0	5.0	6.0	0.448	71.38
29	27.0	3.0	5.0	0.603	68.91
30	20.0	5.0	7.0	0.408	73.32
31	26.0	3.0	9.0	0.478	73.39
32	31.0	4.0	10.0	0.461	77.91
33	23.0	3.0	11.0	0.404	74.66
34	27.0	6.0	5.0	0.475	75.24
35	33.0	4.0	7.0	0.551	75.19
36	24.0	3.0	5.0	0.582	67.85
37	28.0	4.0	11.0	0.402	78.16
38	29.0	5.0	9.0	0.401	78.28
39	32.0	6.0	10.0	0.366	81.86
40	24.0	4.0	7.0	0.464	72.52

This article has been accepted for publication in a future issue of this journal, but has not been fully edited. Content may change prior to final publication.

TABLE 3. ANOVA results for the *Sa* model

So.	SS	MS	F-Value	p-value	Cont. (%)
Model	0.2459	0.0273	46.08	< 0.0001	
S	0.0500	0.1513	252.17	< 0.0001	17.52
I	0.0780	0.1881	313.49	< 0.0001	21.78
L	0.1100	0.2203	367.18	< 0.0001	25.51
SI	0.0025	0.0479	79.88	0.0007	5.55
SL	0.0056	0.0719	119.90	0.0005	8.33
IL	0.0012	0.0336	55.99	0.0009	3.89
S^2	0.0067	0.0767	127.81	0.0006	8.88
I^2	0.0009	0.0288	47.93	0.0009	3.33
L^2	0.0021	0.0450	74.99	0.0007	5.21
Residual	0.0041	0.0006			
Cor Total	0.25				
R^2 = 0.9834; Adjusted R^2 = 0.9753; Predicted R^2 = 0.9678					

TABLE 4. ANOVA results for the *EC* model

So.	SS	MS	F-Value	p-value	Cont. (%)
Model	385.29	42.81	36.82	< 0.0001	
S	79.86	1230.16	1430.42	< 0.0001	23.19
I	139.17	1624.83	1889.33	< 0.0001	30.63
L	169.67	1793.52	2085.49	< 0.0001	33.81
SI	0.54	143.76	167.16	0.0004	2.71
SL	0.38	120.42	140.02	0.0005	2.27
IL	0.23	93.89	109.18	0.0008	1.77
S^2	0.63	150.12	174.56	0.0003	2.83
I^2	0.04	39.25	45.65	0.8427	0.74
L^2	0.33	108.75	126.45	0.0006	2.05
Residual	6.03	0.86			
Cor Total	391.32				
R^2 = 0.9846; Adjusted R^2 = 0.9764; Predicted R^2 = 0.9668					

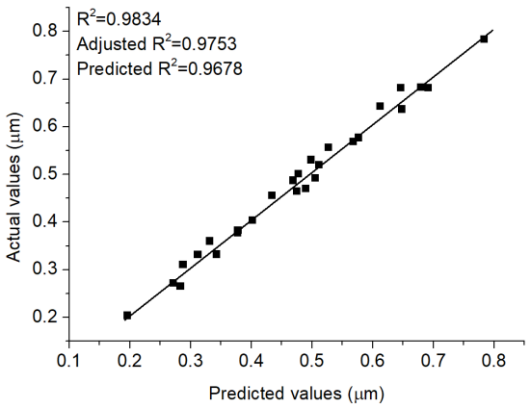

(a) For the *Sa* model

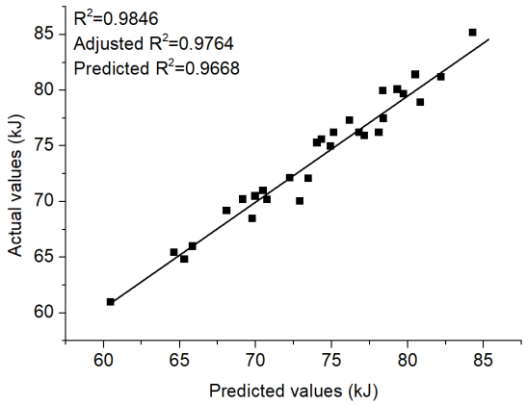

(b) For the *EC* model

Fig. 5. Comparisons between the predictive and actual values

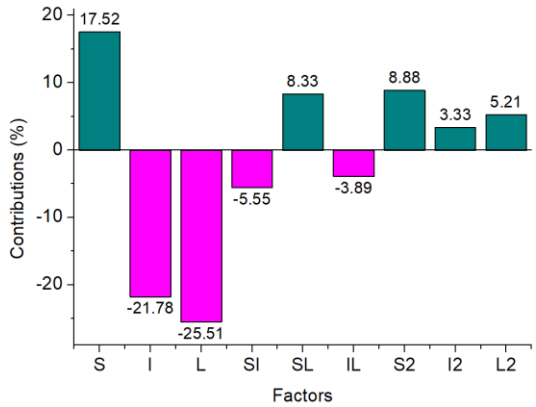

(a) Parametric contributions for the *Sa* model

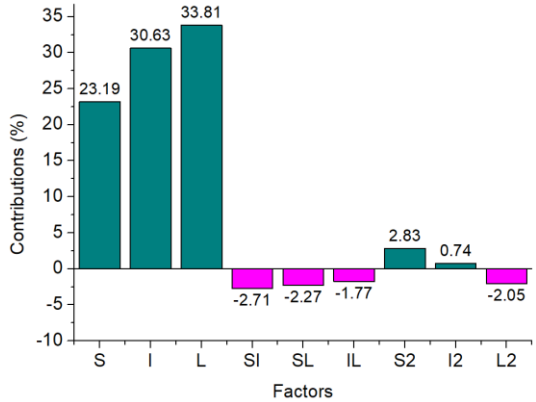

(b) Parametric contributions for the *EC* model

Fig. 6. Parametric contributions for burnishing responses

TABLE 5. Testing results for developed RBFN models

No.	*Sa (μm)*			*EC (KJ)*		
	Exp.	RBFN	Er. (%)	Exp.	RBFN	Er. (%)
28	0.448	0.452	-0.89	71.38	70.92	0.64
29	0.603	0.598	0.83	68.91	69.34	-0.62
30	0.408	0.411	-0.74	73.32	73.86	-0.74
31	0.478	0.473	1.05	73.39	72.98	0.56
32	0.461	0.465	-0.87	77.91	78.24	-0.42
33	0.404	0.408	-0.99	74.66	74.28	0.51
34	0.475	0.471	0.84	75.24	75.48	-0.32
35	0.551	0.554	-0.54	75.19	74.98	0.28
36	0.582	0.586	-0.69	67.85	67.24	0.90
37	0.402	0.405	-0.75	78.16	78.35	-0.24
38	0.401	0.397	1.00	78.28	78.64	-0.46
39	0.366	0.363	0.82	81.86	81.36	0.61
40	0.464	0.468	-0.86	72.52	72.24	0.39

4.2. Parametric impacts

As a result, a higher inlet pressure causes a reduction in the roughness (Fig. 7a). At a low inlet pressure, the temperature of the cold air slightly reduces, resulting in a reduction in the cooling impact. This leads to a higher friction in the burnishing region; hence, the roughness increases. At a high inlet pressure, the temperature of the cold air significantly reduces, leading to lower friction in the burnishing region; hence, a lower roughness is obtained [26].

As a result, a higher CO_2 quantity causes a reduction in the roughness (Fig. 7b). At a high CO_2 quantity, an increased amount of liquid CO_2 is transferred into the interfaces, leading

This article has been accepted for publication in a future issue of this journal, but has not been fully edited. Content may change prior to final publication.

to low friction [19]. The material compression is easily performed; hence, the roughness reduces.

As a result, more energy is consumed with a higher spraying distance (Fig. 8a). At a higher distance between the nozzle and specimen, increased friction is produced due to the low cooling impact [19]. An increase in energy is required to overcome a higher resistance. More energy is consumed with a higher inlet pressure (Fig. 8a). At a higher inlet pressure, cooler air is transferred into the interfaces, leading to higher specimen hardness [20]. An increase in energy is required to process the material.

As a result, more energy is consumed with a higher CO_2 quantity (Fig. 8b). A higher quantity of the liquid CO_2 increases the workpiece's hardness due to an efficient cooling impact [21]. A higher amount of energy is consumed to compress the specimen.

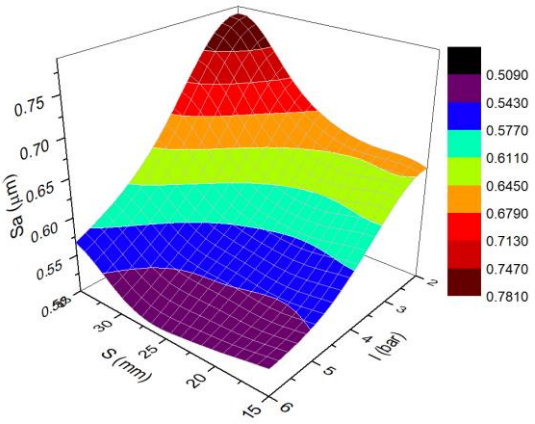

(a) *Sa* versus *S and I*

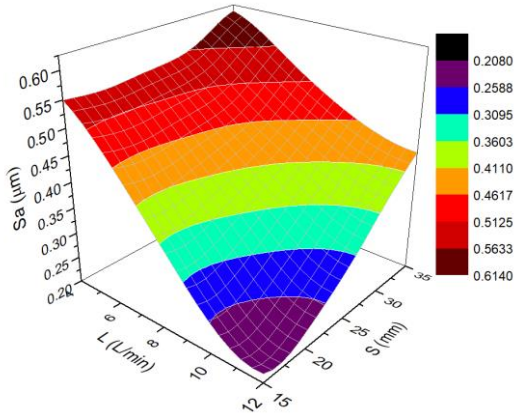

(b) *Sa* versus *S and L*

Fig. 7. The main impacts of process parameters on the *Sa*

4.3. The optimal results

The computed weights of the *Sa* and *EC* are 0.63, and 0.37, respectively. Fig. 9 shows the Pareto graphs produced by IGWO. As a result, a low energy has corresponded with a higher roughness. The best solution is selected using the TOPSIS. As a result, the optimal *S*, *I*, and *L* are 15.0 mm, 3.0 bar, and 11.0 L/min, respectively. At the selected solution, the *Sa* and *EC* are reduced by 20.4% and 3.8%, respectively (Table 6).

The NSGA-II and TOPSIS are utilized to find optimal factors. As a result, the optimal *S*, *I*, and *L* are 15.0 mm, 2.0 bar, and 12.0 L/min, respectively (Table 6). The *Sa* and *EC* are reduced by 13.3% and 2.9%, respectively. It was pointed out that the IQWO provided better optimal results, as compared to the NSGA-II.

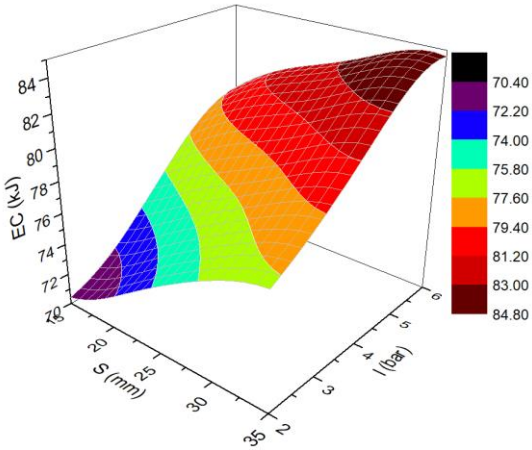

(a) *EC* versus *S and I*

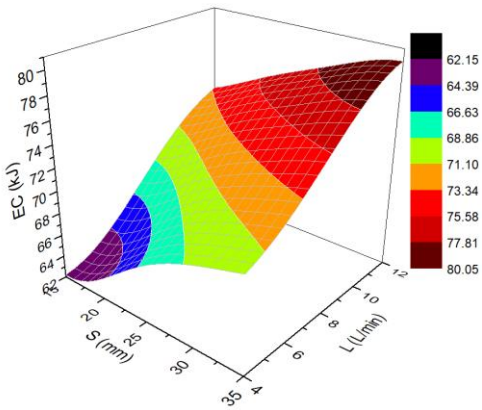

(b) *EC* versus *S and L*

Fig. 8. The main impacts of process parameters on the *EC*

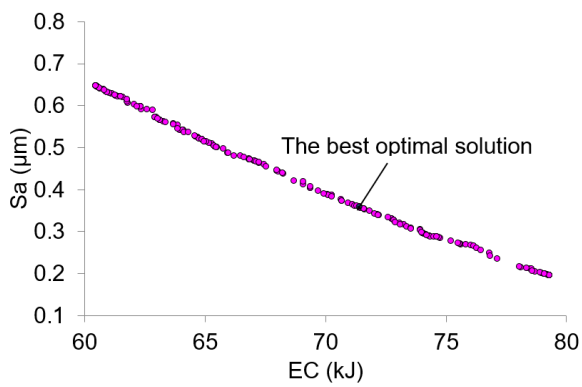

Fig. 9. Pareto fronts produced by the IGWO

This article has been accepted for publication in a future issue of this journal, but has not been fully edited. Content may change prior to final publication.

TABLE 6. Optimization results produced by the IGWO and NSGA-II

Method	*S* (mm)	*I* (bar)	*L* (L/min)	*Sa* (μm)	*EC* (kJ)	E_I
Initial results	25.0	4.0	8.0	0.441	74.02	
IQWO	15.0	3.0	11.0	0.351	71.22	0.884
Reductions by the IQWO (%)				-20.4	-3.8	
NSGA-II	15.0	2.0	12.0	0.382	71.86	0.832
Reductions by the NSGA-II (%)				-13.3	-2.9	

5. CONCLUSIONS

In this investigation, a cool and cryogenic-assisted diamond burnishing operation was developed and optimized. The reductions in the roughness and energy consumed were obtained using optimal *S*, *I*, and *L*. The RBFN, IGWO, NSGA-II, and TOPSIS were utilized to propose burnishing responses and select the optimality. The conclusions can be expressed as:

1. A lower spraying distance could be used to minimize the *Sa* and *EC*. Higher inlet pressure and CO_2 quantity could be applied to reduce the *Sa*. The lower inlet pressure and CO_2 quantity could be applied to save *EC*.
2. In terms of the *Sa* and *EC* models, the CO_2 quantity had the highest contribution, followed by the inlet pressure and spraying distance, respectively.
3. The optimal *S*, *I*, and *L* generated by the IGWO were 15.0 mm, 3.0 bar, and 11.0 L/min, respectively. The reductions in the *Sa* and *EC* were 20.4% and 3.8%, respectively.
4. The optimization approach can be effectively used to solve optimizing issues for different burnishing processes.
5. The BRFN approach can be employed to present non-linear relations of experimental data.
6. The developed cooling system can be effectively employed to facilitate other burnishing operations without any lubricants.
7. The developed burnishing operation can be utilized to produce surface finishing for interior holes.
8. The designed and fabricated tool can be utilized in other internal diamond burnishing operations.
9. To improve the roughness and energy efficiency of the practical diamond burnishing operation, optimal parameters and responses can be utilized.
10. The investigation's results can be used to create an intelligent system that will enable the internal diamond burnishing operation across a range of industries.
11. The impacts of the process parameters on the hardness and the depth of the affected layer will be explored in future works.

REFERENCES

[1] O. Taamallah, H. Hamadache, N. Mokas, A. Amirat,, B. Hamadi, "Investigation of the effects of slide diamond burnishing process on the mechanical performance of GCr15 steel," *J. Fail. Anal. and Preven.*, vol. 23, pp. 1101–1113, 2023, doi: 10.1007/s11668-023-01652-5.

[2] R. Kluz, M. Bucior, A. Dzierwa, K. Antosz, W. Bochnowski, K. Ochał, "Effect of diamond burnishing on the properties of FSW joints of EN AW-2024 aluminum alloys," *Appl. Sci.*, vol. 13, no. 2, pp. 1305, 2023, doi: 10.3390/app13031305.

[3] T. T. Nguyen and A. L. Van, "Machining and optimization of the external diamond burnishing operation," *Mater. Manuf. Process.*, vol. 38, no. 10, pp. 1276–1290, 2023, doi: 10.1080/10426914.2022.2072880.

[4] B. Sachin, S. Narendranath, D. Chakradhar, "Application of desirability approach to optimize the control factors in cryogenic diamond burnishing," *Arab. J. Sci. Eng.*, vol. 45, pp. 1305–1317, 2020, doi: 10.1007/s13369-019-04326-3.

[5] [5] J. Zaghal, V. Molnar, M. Benke, "Improving surface integrity by optimizing slide diamond burnishing parameters after hard turning of 42CrMo4 steel;" *Int. J. Adv. Manuf. Technol.*, vol. 128, pp. 2087–2103, 2023, doi: 10.1007/s00170-023-12008-6.

[6] C. Felhő and G. Varga, "CAD and FEM modelling of theoretical roughness in diamond burnishing," *Int. J. Precis. Eng. Manuf.*, vol. 23, pp. 375–384, 2022, doi: 10.1007/s12541-022-00622-5.

[7] T. T. Nguyen, T. A. Nguyen, A. L. Van, X. B. Dang, "Multi-performance optimization of the diamond burnishing process in terms of energy saving and tribological factors," *Proc. Inst. Mech. Eng. E: J. Process Mech. Eng.*, online first, 2023. doi:10.1177/09544089231163407.

[8] J. Maximov, G. Duncheva, A. Anchev, V. Dunchev, Y. Argirov, "Improvement in fatigue strength of chromium–nickel austenitic stainless steels via diamond burnishing and subsequent low-temperature gas nitriding," *Appl. Sci.*, vol. 14, no. 3, pp. 1020, 2024, doi: 10.3390/app14031020.

[9] G. V. Duncheva, J. T. Maximov, A. Anchev, V. Dunchev, Y. Argirov, S. Velkov, "Modeling and optimization of surface integrity and sliding wear resistance of diamond-burnished holes in austenitic stainless steel cylinder lines," *Machines*, vol. 11, pp. 872, 2023, doi: 10.3390/machines11090872.

[10] T. Ouahiba, H. Hamid, B. Selma, L. Laouar, "Multi-objective optimization of slide diamond burnishing parameters for enhanced fatigue resistance of AISI 52100 steel," *J. Braz. Soc. Mech. Sci. Eng.*, vol. 46, pp. 451, 2024, doi:10.1007/s40430-024-05001-x.

[11] J. T. Maximov, G. V. Duncheva, "Effects of cryogenic- and cool-assisted burnishing on the surface integrity and operating behavior of metal components: A review and perspectives". *Machines*, vol. *12*, pp. 312, 2024; doi: 10.3390/machines12050312.

[12] J. Chodór, L. Kukiełka, G. Chomka, L. Bohdal, R. Patyk, M. Kowalik, T. Trzepieciński, A. M. Radchenko, "Using the FEM method in the prediction of stress and deformation in the processing zone of an elastic/visco-plastic material during diamond sliding burnishing," *Appl. Sci.*, vol. 13, no. 3, pp. 1963, 2023, doi: 0.3390/app13031963.

[13] S. C. Cagan, M. Maci, M. M. Buldum, C. Maci, "Artificial neural networks in mechanical surface enhancement technique for the prediction of surface roughness and microhardness of magnesium alloy," *Bull. Polish Acad. Sci. Tech. Sci.*, vol. 67, pp. 729-739, 2019, doi: 10.24425/bpasts.2019.130182.

[14] P. Zhou and M. Tan, "Robust zeroing neural networks with two novel power-versatile activation functions for solving dynamic Sylvester equation," *Bull. Polish Acad. Sci. Tech. Sci.*, vol. 70, pp. e141307, 2022, doi: 10.24425/bpasts.2022.141307.

[15] Q. Chenghui, W. Chongtian, Y. Xiaolu, W. Linxu, Y. Jiaming, S. Hong, "Multi-objective optimization of PCM-fin structure for staggered Li-ion battery packs", Bull. Polish Acad. Sci. Tech. Sci., vol. 71, no. 4, pp. e145677, 2023, doi: 10.24425/bpasts.2023.145677.

[16] A. Saldaña-Robles, H. Plascencia-Mora, E. Aguilera-Gómez, A. Saldaña-Robles, A. Marquez-Herrera, J. A. Diosdado-De la Peña, "Influence of ball-burnishing on roughness, hardness and corrosion resistance of AISI 1045 steel", *Surf. Coat. Technol.*, vol. 339, pp. 191–198, 2018, doi:10.1016/j.surfcoat.2018.02.013.

[17] B. Buldum, S. Cagan, "Study of ball burnishing process on the surface roughness and microhardness of AZ91D Alloy", *Exp. Tech.*, vol. 42, pp. 233–241, 2018, doi:10.1007/s40799-017-0228-8.

[18] G. D. Revankar, R. Shetty, S. S. Rao, V. N. Gaitonde, "Analysis of surface roughness and hardness in ball burnishing of titanium alloy", Measurement, vol. 58, pp. 256–268, 2014, doi:10.1016/j.measurement.2014.08.043.

[19] M. T. Le, A. L. Van, T. T. Nguyen, X. B. Dang, "Ecological design optimization of nozzle parameters for burnishing operation", *J. Appl. Eng. Sci.*, vol. 21 (2), pp. 686-697, 2023, doi: 10.5937/jaes0-41943.

[20] T.T. Nguyen, T.A. Nguyen, Q. H. Trinh, X. B. Le, "Multi-performance optimization of multi-roller burnishing process in sustainable

This article has been accepted for publication in a future issue of this journal, but has not been fully edited. Content may change prior to final publication.

lubrication condition", *Mater. Manuf. Process.*, vol. 37(4), pp. 407–427, 2021, doi: 10.1080/10426914.2021.1962533.

[21] B. Huang, Y. Kaynak, Y. Sun, I. S. Jawahir, "Surface Layer modification by cryogenic burnishing of Al 7050-T7451 alloy and validation with FEM-based burnishing model", *Procedia CIRP*, vol. 31, pp. 1-6, 2015, doi: 10.1016/j.procir.2015.03.097.

This article has been accepted for publication in a future issue of this journal, but has not been fully edited. Content may change prior to final publication.